NANO · MICRO small
www.small-journal.com

Bioinspired Nacre-Like Alumina with a Metallic Nickel Compliant Phase Fabricated by Spark-Plasma Sintering

*Amy Wat, Claudio Ferraro, Xu Deng, Andrew Sweet, Antoni P. Tomsia, Eduardo Saiz, and Robert O. Ritchie**

Many natural materials present an ideal "recipe" for the development of future damage-tolerant lightweight structural materials. One notable example is the brick-and-mortar structure of nacre, found in mollusk shells, which produces high-toughness, bioinspired ceramics using polymeric mortars as a compliant phase. Theoretical modeling has predicted that use of metallic mortars could lead to even higher damage-tolerance in these materials, although it is difficult to melt-infiltrate metals into ceramic scaffolds as they cannot readily wet ceramics. To avoid this problem, an alternative ("bottom-up") approach to synthesize "nacre-like" ceramics containing a small fraction of nickel mortar is developed. These materials are fabricated using nickel-coated alumina platelets that are aligned using slip-casting and rapidly sintered using spark-plasma sintering. Dewetting of the nickel mortar during sintering is prevented by using NiO-coated as well as Ni-coated platelets. As a result, a "nacre-like" alumina ceramic displaying a resistance-curve toughness up to ≈16 MPa $m^{1/2}$ with a flexural strength of ≈300 MPa is produced.

The remarkable damage-tolerance found in natural materials is developed through functional, multiscale architectures with structural gradients and graded interfaces.[1–6] One notable example is nacre, which comprises ceramic (mineral) platelets of polycrystalline aragonite (≈95% by volume) bonded by biopolymers in a "brick-and-mortar" structure.[1,3,7] The mineral platelets in this structure impart high strength whereas the organic mortar acts as compliant layer to create ductility by permitting platelet sliding which dissipates locally high stresses. To maintain strength, such sliding is limited to a few micrometers by such mechanisms as frictional resistance from the surface roughness of the platelets,[8] the tensile/shear resistance of the biopolymer interphase,[9] the presence of preexisting interlayer bridges,[10,11] and in certain species the dovetail geometry of the platelets.[12] Toughening is generated extrinsically,[13] primarily by crack bridging leading to brick pull-out and crack-path deflection,[14] to an extent that the fracture toughness of nacre (in energy terms) is several thousand times higher than that of its constituents.

There has been great interest in mimicking this nacre-like structure to generate high-toughness ceramics. Processing techniques such as freeze-casting (ice templating),[15–23] layer-by-layer alignment,[24,25] thermal spray processing,[26] sedimentation,[27] coextrusion,[28,29] magnetic platelet alignment, and vacuum filtration assisted alignment[24,30] have been used to recreate brick-and-mortar microstructures. Using polymeric mortars, the nacre-like ceramics avoid sudden catastrophic failure by stabilizing slow crack growth in the form of crack-resistance (R-curve) behavior, although they cannot be used at elevated temperatures due to the presence of polymer phase.[20,24–27,31,32] Theoretical micromechanical modeling[33] of synthetic "brick-and-mortar" materials has indicated that metallic mortars may permit higher-temperature operation while further enhancing the strength and toughness properties due to their higher shear/tensile strength (provided the mortar strength does not exceed the brick strength).[34] However, to realize the full effect of a metallic mortar, the bonding between the mortar and the bricks must be strong enough so that the vital interbrick displacements are *within* the mortar, and not along the brick–mortar interfaces. Moreover, processing such hybrid ceramics with a metallic compliant phase is difficult as metals do not generally wet ceramics and thus cannot be readily melt-infiltrated into a (e.g., freeze-cast) ceramic scaffold. [35–37]

To avoid this issue, in this study we have developed a "bottom-up approach" to create fine-scale, high volume fraction (≈95%) alumina brick-and-mortar structures with an ≈5%

Dr. A. Wat, Dr. A. P. Tomsia, Prof. R. O. Ritchie
Materials Sciences Division
Lawrence Berkeley National Laboratory
Berkeley, CA 94720, USA
E-mail: roritchie@lbl.gov
Dr. A. Wat, A. Sweet, Prof. R. O. Ritchie
Department of Materials Science and Engineering
University of California
Berkeley, CA 94720, USA
Dr. C. Ferraro, Prof. E. Saiz
Center for Advanced Structural Ceramics
Department of Materials
Imperial College London
London SW7 2AZ, UK
Prof. X. Deng
Institute of Fundamental and Frontier Sciences
University of Electronic Science and Technology of China
Chengdu 610054, China
The ORCID identification number(s) for the author(s) of this article can be found under https://doi.org/10.1002/smll.201900573.

DOI: 10.1002/smll.201900573

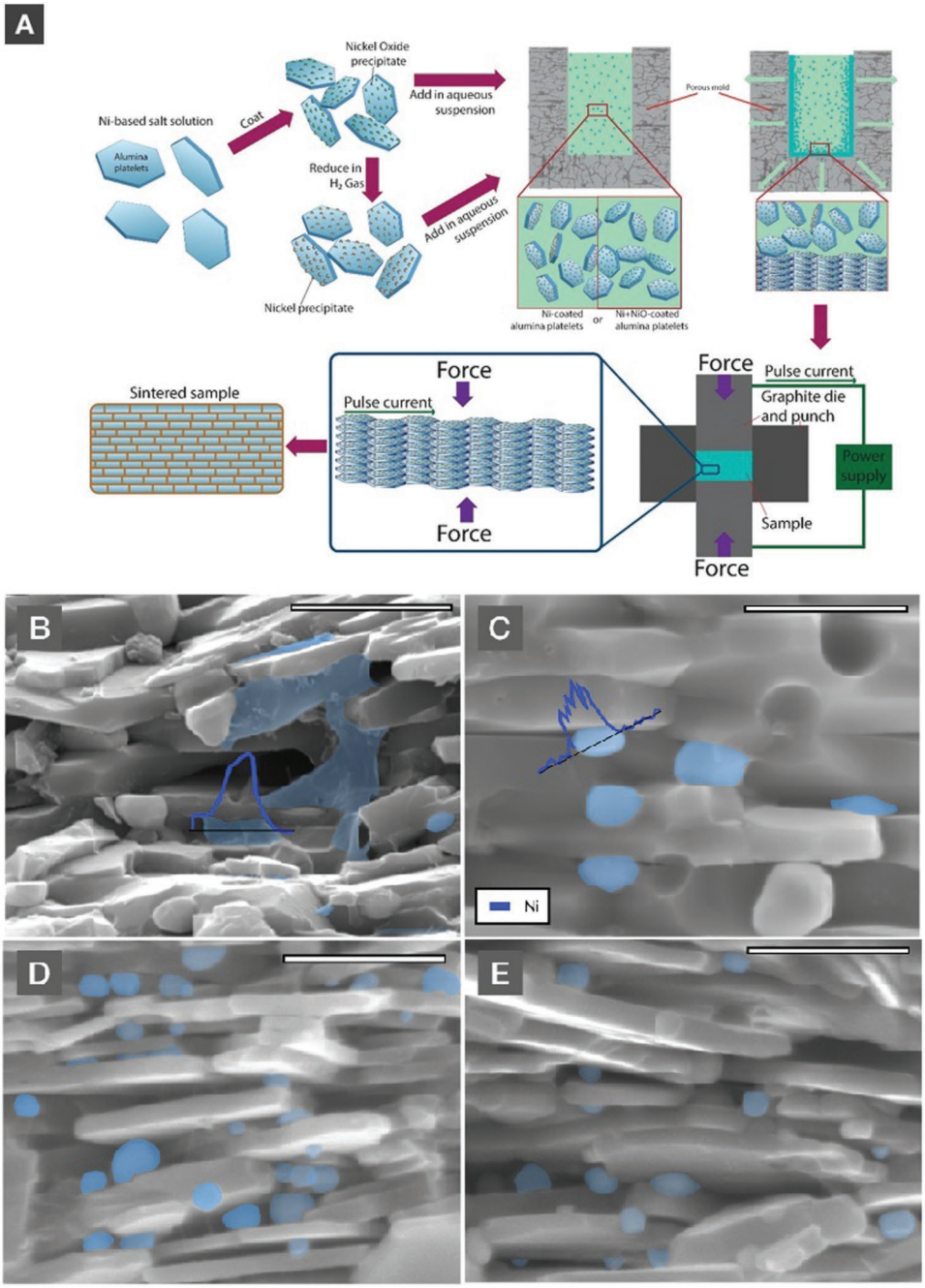

Figure 1. A) Flow chart summarizes the "bottom-up" processing to create nacre-like (brick-and-mortar) alumina structures. SEM images illustrate the nature of the nickel-phase "mortar" formed within Ni+NiO-coated alumina and Ni-coated alumina samples with 5 µm scale bars. In the Ni+NiO-coated samples, sintering at B) 1100 °C generates a sheet of nickel that sits between the alumina platelets, whereas sintering at C) 1200 °C causes the nickel to dewet and act as ball-shaped impurities in the alumina. D,E) For the Ni-coated materials, nickel dewets at both sintering temperatures, 1100 and 1200 °C. The blue lines are EDS line scan results to show changes in nickel content.

nickel (mortar) compliant phase in the true image of nacre. We achieved this by coating high aspect ratio, 0.5–1 µm thick, alumina platelets (comparable in size to the mineral platelets in natural nacre) with nickel oxide or nickel,[38] which were then aligned using slip-casting prior to spark-plasma sintering (SPS) at 1100 or 1200 °C, as summarized in **Figure 1**A. Details of the processing are given in the Experimental Section.

Nickel is an ideal metallic mortar because of its high melting point, strength, and ductility, but for it to function as a reliable compliant phase surrounding the alumina bricks in the final nacre-like structure, it must not completely dewet from the ceramic. To achieve this, we used both nickel- and nickel oxide-coated platelets (the coating procedures are described in Figure S1, Supporting Information). Accordingly, two batches

of materials were cast: one made solely with Ni-coated platelets, the other with a mixture of NiO-coated and Ni-coated platelets. By examining their fracture surfaces (Figure S2, Supporting Information), it was apparent that slip-casting had successfully aligned the Ni+NiO-coated alumina platelets, and SPS at 1100 and 1200 °C had completely sintered the materials into a micrometer-scale brick-and-mortar structure with a low nickel content of ≈5 wt% (below 1100 °C, the samples did not fully sinter). Note that SPS was not used to sinter the ceramic platelets per se but rather to sinter the Ni or NiO coatings on the platelets without dewetting in order to create samples with individual alumina "bricks" held together by consolidated nickel "mortar" to properly replicate the toughening mechanisms observed in its natural counterpart. The role of nickel oxide coatings was critical in limiting the extent of dewetting by the nickel phase during sintering because controlled increases in oxygen concentration can decrease the wetting angle without any reaction at the interface, despite a heavily reducing graphite environment under vacuum.[35] Specifically, the addition of oxygen lowers the surface energy of Ni and its contact angle with alumina, which reduces the interfacial energy between alumina and nickel and possibly the surface energy of alumina itself.[35,39] This reduction in surface energy is caused by adsorption or excess oxygen in the different interfaces (the surface of Ni and the Ni–Al_2O_3 interface).[40] Materials sintered at 1100 °C from Ni+NiO-coated platelets did show limited signs of nickel dewetting (Figure 1B). However, those sintered at 1100 °C from solely Ni-coated platelets (Figure 1D), and at ≥1200 °C for both Ni+NiO-coated and Ni-coated platelets (Figure 1C,E), were subject to extensive dewetting, with small agglomerates of nickel forming between the alumina platelets (sintering at >1200 °C additionally resulted in alumina grain growth). The Ni samples sintered at 1100 and 1200 °C displayed limited sintering between platelets as the alumina brick dimensions were $0.52 \pm 0.15 \times 6.6 \pm 2.1$ and $0.54 \pm 0.15 \times 5.1 \pm 1.2$ μm, respectively. The Ni+NiO samples also displayed limited sintering between platelets at 1100 and 1200 °C, with alumina brick dimensions were $0.88 \pm 0.35 \times 6.1 \pm 1.8$ and $1.6 \pm 0.\ 5 \times 6.7 \pm 2.4$ μm, respectively. Energy-dispersive X-ray spectroscopy of these surfaces (Figure 1B,C) confirmed the larger aggregations of nickel in samples sintered at 1200 °C, compared to the sheets of nickel when sintered at 1100 °C. This became very pronounced when the Ni+NiO-alumina samples were sintered at 1300 °C (Figure S3a, Supporting Information).

The mechanical properties of the compliant-phase Ni-alumina and Ni+NiO-alumina ceramics, sintered at 1100 and 1200 °C, were evaluated with respect to their flexural strength and fracture toughness and compared with the corresponding properties of fine-grained monolithic alumina. The flexural strength of alumina can vary between 267 and 358 MPa due to variations in grain size or sample size.[41] The flexural strength of our materials was comparable to this (**Figure 2**A); the mean strength of our Ni+NiO-alumina sintered at 1100 °C was 297.1 ± 43.1 MPa (some samples displayed strengths as high as ≈350 MPa), whereas the corresponding strength of our Ni+NiO-alumina sintered at 1200 °C was ≈17% lower at 246.5 ± 30.4 MPa. When extensive dewetting of nickel occurred, as in the Ni-alumina sintered at 1100 and 1200 °C (Figure 1D,E), the metal–ceramic interfaces are weakened from Ni dewetting such that the mean flexural strengths decreased several-fold to ≈85± 9.15 and ≈118 ± 19.3 MPa, respectively.

Whereas the strength does not vary much between monolithic alumina and our (appropriately sintered) compliant-phase alumina, the fracture toughness shows stark differences. All the Ni-alumina samples fractured catastrophically at a particularly low toughness without any evidence of stable crack growth, that is, no R-curve behavior (Figure 2B). Specifically, Ni-coated samples sintered at 1100 and 1200 °C, again where extensive Ni dewetting was observed (Figure 1D,E), had average fracture toughness values of 1.20 ± 0.05 and 2.55 ± 0.21 MPa $m^{½}$, respectively. These values are even less than those reported for monolithic alumina.[42–44]

Clearly, the most critical aspect of processing the compliant-phase aluminas here to attain damage-tolerance is to minimize the dewetting of the Ni mortar. As noted above, we can achieve this through the use of 1100 °C-sintered NiO-coated alumina platelets as this dramatically increases the fracture toughness. Instead of fracturing catastrophically, the Ni+NiO-coated alumina sintered at 1100 °C displays stable crack-growth behavior, as indicated by the rising R-curve behavior in Figure 2B, which doubles the toughness from ≈7.8 MPa $m^{½}$ at crack initiation to 15.9 MPa $m^{½}$ after ≈250 μm of slow crack growth. Such R-curve behavior represents a sixfold increase in fracture toughness compared to samples sintered at 1200 °C, which suffer sudden catastrophic fracture at 2.48 ± 1.10 MPa $m^{½}$ with no evidence of rising R-curve behavior. Indeed, the compliant-phase Ni+NiO-coated alumina sintered at 1100 °C is ≈2–4 times tougher than monolithic alumina (at a comparable flexural strength).

The other key to successful processing of this high-toughness Ni+NiO-coated alumina is spark-plasma sintering; by applying high pressures and rapid heating rates (exceeding 300 °C min^{-1}, compared to conventional heating at typically ≈20 °C min^{-1}), with the goal of sintering only the nickel coating of the alumina platelets together while grain growth and sintering of alumina is suppressed to maintain the desired high aspect ratio of the ceramic platelets.[45,46] Scanning electron microscopy (SEM) images of the fracture surfaces in Figure 1C show that the nickel in the Ni+NiO-alumina samples showed only limited dewetting when sintered at 1100 °C. Indeed, the stretched and torn pieces of nickel shown in Figure 2C,D imply that the interbrick displacements, and hence the fracture path in these materials, occurred *within* the nickel mortar layers, which is significant for obtaining optimal toughness. This was the result of the rapid sintering with SPS, the pressure aiding flow of melted nickel, and wetting from increased oxygen content from the NiO coatings.

Sintering at, or above, 1200 °C was clearly detrimental because the Ni dewets excessively forming balls of metal, despite the addition of NiO-coated platelets. A contributing factor here is the highly reducing SPS atmosphere which can deplete oxygen in the system at higher temperatures, making it difficult to prevent nickel dewetting. Essentially, the platelets sinter together to form a material that is best described as alumina with a long-grained microstructure and nickel-based inclusions. As such, the nickel no longer functions as a compliant phase and introduces defects into the alumina, leading to strengths and toughnesses that are lower than monolithic alumina.

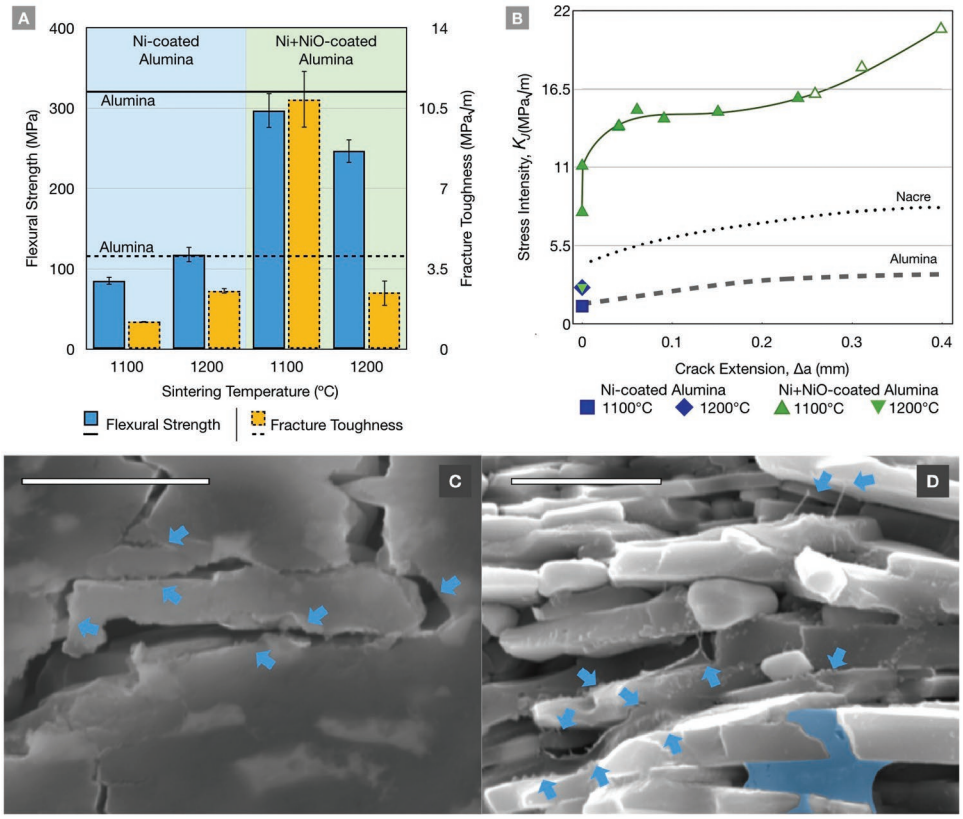

Figure 2. A) Summarized mechanical testing results in bar graphs, showing flexural strength and fracture toughness test results. B) The Ni+NiO-coated samples sintered at 1100 °C show R-curve behavior that enhances the fracture toughness of the material from ≈8 to 16 MPa $m^{½}$ associated with slow (stable) crack growth, toughness behavior that is far superior to that of fine-grained monolithic alumina (and even nacre). In contrast, the samples sintered at 1200 °C or with only Ni-coated platelets display no R-curve behavior and fracture catastrophically with a fracture toughness lower than alumina. The unfilled points are data points that are not strictly "valid" according to ASTM Standard E1820 because they exceed the maximum crack extension for the size of the test specimens. SEM images with 5 µm scale bars illustrate the salient toughening mechanisms in the Ni+NiO-coated alumina samples sintered at 1100 °C. C) Although there is some Ni dewetting based on the brighter areas, evidence of nickel tearing (highlighted by blue arrows) and ceramic "brick" pull-out are observed along crack path. D) The fracture surface shows more signs of nickel tearing in between the platelets, indicated by the blue arrows, with untorn nickel in the blue region. This suggests that the interbrick displacements and the resulting fracture paths may occur *within* the nickel mortar phase rather than along the Al_2O_3–ceramic/Ni–metal interfaces.

In contrast, the Ni+NiO alumina materials, spark-plasma sintered at 1100 °C, displayed no marked change in the size/shape of the ceramic bricks (at widths of 0.882 ± 0.345 µm and lengths of 6.06 ± 1.8 µm) with a distributed nickel phase along the ceramic–brick interfaces. This allows for limited interbrick displacements—the key mechanistic feature for toughness in nacre-like materials—through the plasticity of the mortar phase. The role of the NiO coating is crucial here. Although SPS is powerful due to its rapid sintering capabilities and continuous applied pressure, the nickel can dewet when cooling at the end of the sintering process. The "sheet" of Ni between the bricks was only possible due to the addition of NiO-coated alumina platelets, which prevents the dewetting of nickel. As a result, we attained fully dense samples with a coating of nickel acting as the mortar between the bricks. By allowing the material to display brick pull-out, mortar phase tearing, crack bridging and deflection, as observed in nacre (**Figure 3**B,C), SPS processing at 1100 °C with NiO-coated platelets generates an impressive ceramic with a flexural strength on the order of monolithic (untoughened) alumina but with a toughness some 2–4 times higher.

While a marked improvement in the toughness of alumina has been achieved without loss in strength, micromechanical modeling[33] suggests that the damage-tolerance of these nacre-like ceramics materials may be further improved. As noted above, the evidence in Figure 2C,D suggests that the interbrick displacements in the Ni+NiO alumina occur within the metallic mortar phase rather than along the brick/mortar interfaces, but this may not be always the case. Since the nickel layers are very thin and at times discontinuous (Figure S3b, Supporting Information), the nickel may not act as a completely effective "lubricating" layer between the platelets. This issue still remains the "Achilles heel" of brick-and-mortar ceramic structures; obtaining an effective metallic mortar with strong bonding to the ceramic bricks has yet to be completely realized. Without further study to produce an effective mortar between the platelets, the potential for high-temperature applications for these materials have not been fully achieved. This remains the grand

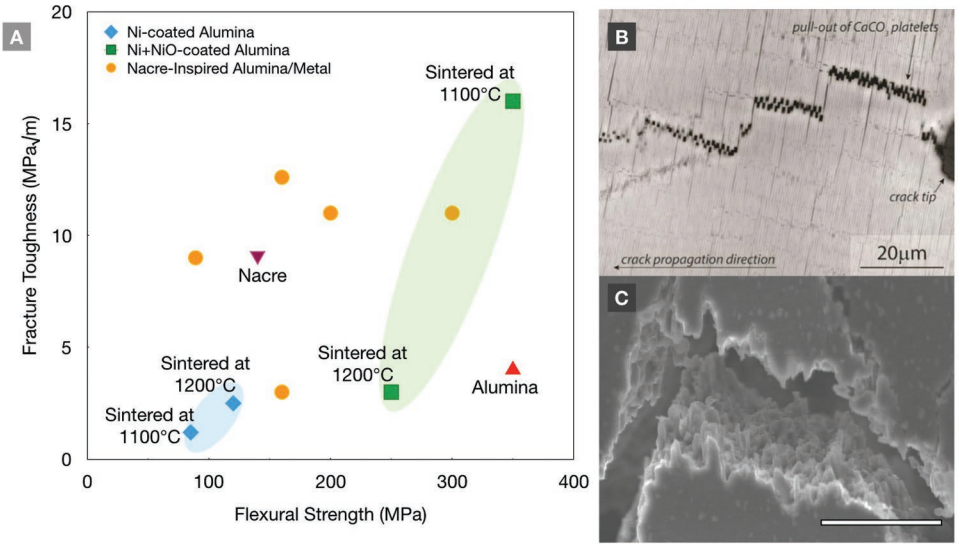

Figure 3. A) Comparison of reported mechanical properties of bioinspired (nacre-like) alumina ceramics containing less than 10 vol% metallic mortar, taken from refs. [23,24,29,47,48] (circular data points), with that of nacre (triangular data point) and the current results (square and diamond data points) to illustrate how the composition, processing, and sintering temperature can affect their damage-tolerance (strength and toughness). B,C) Scanning electron microscopy image of the path of a crack in natural nacre and Ni+NiO-coated alumina sintered at 1100 °C (with a 25 μm scale bar), shows toughening via the pull-out of the platelets (with displacements in the range of a few micrometers) leading to crack bridging, the coarser-scale defection of the crack path, roughly perpendicular to orientation of the platelets, and the corresponding formation of a rough fracture surface as the crack tried to maintain a macroscopic path nominally perpendicular to the applied tensile stress. Image (B) courtesy of Bernd Gludovatz.

challenge in the development of new bioinspired lightweight structural materials in the image of natural nacre.

Nevertheless, the results of this work illustrate the criticality of controlling metal wetting to create damage-tolerant ceramics with a metallic phase, for example, through the use here of NiO- as well as Ni-coated alumina with rapid 1100 °C SPS sintering. The mechanical properties of our Ni+NiO-alumina ceramics have high damage-tolerance relative to other bioinspired ceramics with a <10 vol% metallic phase (Figure 3A). For example, a similar approach was used in a previous study,[47] but the reported toughness values were an order of magnitude lower than the ceramics developed here, which may have originated from poor bonding between the ceramic and metallic phases (NiO-coatings were not employed). Slip-casting or freeze-casting has also been used to process alumina/copper[48] and alumina/nickel materials,[47,49] and freeze-casting has been employed to align Ni-coated alumina platelets prior to hot pressing,[49] but in all these cases the resulting toughnesses were significantly lower than the materials developed here, we presume due to extensive dewetting of the metallic phase. The work of Garnier and Dunand[49] is notable for its use of freeze-casting to make nickel-alumina composites but these did not replicate the structure and key mechanistic features of nacre due to the their high (≈30 wt%) nickel content, large nickel agglomerates (with diameters up to 6 μm) and consequent restricted brick sliding which compromises toughness. Coextrusion has also been used to create nacre-like structures with high volume fractions of ceramic and a metallic mortar, but these structures tend to be far coarser, with brick thicknesses of hundreds of micrometers; this results in good toughnesses up to ≈11 MPa $m^{1/2}$, but very low flexural strengths of 110–160 MPa.[28,29]

Indeed, we believe that our Ni+NiO-alumina is the first nacre-like ceramic with a metallic mortar displaying a flexural strength comparable to monolithic alumina (≈300 MPa) but with a several-fold increase in fracture toughness up to ≈16 MPa $m^{1/2}$ (associated with rising R-curve behavior), a material made possible by controlling the wetting of Ni using rapid spark-plasma sintering of slip-casting of NiO-coated and Ni-coated alumina platelets at the appropriate temperature. The authors speculate that the limited dewetting was feasible at lower temperatures because slower diffusion and incomplete reduction of NiO leads to more oxygen activity at the interface between the Ni and alumina to form a lower contact angle. The limited dewetting of the nickel mortar phase and stronger bonding between the metallic mortar and the ceramic bricks are critical for imparting high strength and fracture toughness within bioinspired ceramics because this ensures that the crucial interbrick displacements and energy dispersion at stress concentrators occur *within* the mortar. These components have generally been overlooked in the scientific community's past efforts to mimic the remarkable combinations of strength and fracture toughness found in natural materials.

Experimental Section

The starting material in the form of 0.5–1 μm thick, 5–7 μm wide alumina platelets (Alusion, Antaria Limited, Australia) was coated with a nickel or nickel oxide shell using a coating procedure modified from Shen et al.[38] Further details are given in the Supporting Information and are illustrated in Figure S1 (Supporting Information). Slip-casting of slurries was then employed, with ≈50 wt% solid loading, to align the platelets in order to produce green bodies with a high packing density. To learn how to control the nickel wetting behavior on the ceramic platelets,

slurries with two different compositions were prepared for sintering: one with only Ni-coated platelets and another with a mixture of 20 wt% NiO- and 80 wt% Ni-coated alumina platelets. The suspensions, which contained 10 vol% polyvinyl alcohol (PVA) 22000 (VWR, Belgium) and 4 vol% Dolapix CA (Zschimmer & Schwarz, Germany) to aid with green body strength and dispersion, were manually stirred and degassed in vacuo. The suspensions were mixed with 63 vol% water using a Thinky ARE-250 planetary mixer for 2 min at 2000 revolutions min^{-1} and 800 rotations min^{-1} with 2 min degassing between mixing steps. The slurries were poured into a mold to settle, dried at 37 °C for 24 h, and baked at 100 °C for 48 h. The polymer binder in the pellets was burnt out in argon at 500 °C for 1 h at 1 °C min^{-1} in a graphite furnace (FCT Systeme, Effelder-Rauenstein, Germany). The materials were sintered using an SPS furnace (HPD 25/1 furnace, FCT Systeme, Germany). They were compressed under vacuum at 55 MPa and heated to 1100 and 1200 °C for 10 min between two graphite punches inside a 20 mm diameter, cylindrical graphite die, before slowly cooling to room temperature. Densities were measured using the Archimedes method. A cross section of the aligned alumina platelets after uniaxial pressing is shown in Figure S1 (Supporting Information).

To prepare for microstructural characterization and mechanical testing, the sintered samples were cut perpendicular to the aligned direction with a diamond-coated saw and carefully polished using diamond grinding discs with a final polish at 0.5 µm. The resulting 12 mm long beams for flexural strength and fracture toughness testing had a square cross section of ≈2.5 × 2.5 mm with a length of 12 mm, in general accordance with the respective ASTM D790[50] and ASTM E1820[51] Standards. Flexural strength was measured on three unnotched samples for each processing condition in three-point bending (with a loading support span of 10 mm) on an Instron 5944 electromechanical testing system (Instron Corporation, Norwood, MA) at a displacement rate of 1 µm s^{-1}.

Corresponding fracture toughness measurements were conducted on three single edged-notched bend SEN(B) samples for each processing condition. The notches were made using a low-speed diamond saw and sharpened by polishing the root with a razor blade immersed in a 6 µm diamond slurry under a steady load. The resulting root radii of the notches averaged between 6 and 20 µm. The samples were tested with an in situ Deben MicroTest 2kN (Deben, UK) three-point bending apparatus with a 10 mm loading span at a displacement rate of 0.55 µm s^{-1} mounted inside a Hitachi S-4300SE/N (Pleasanton, CA) SEM measuring the crack-initiation fracture toughness and any subsequent subcritical crack growth, that is, the crack resistance or R-curve, while simultaneously measuring the crack path and imaging in real time the interaction of this path with the microstructural features. Since these materials display some inelasticity, nonlinear-elastic fracture mechanics measurements were used to find *J*-based crack resistance curves, where *J* is the *J*-integral, which describes the local nonlinear-elastic stress at the crack tip of a nonlinear material. The standard mode I *J*–*K* equivalence was used to find the equivalent stress-intensity values for each data point. Further details for the calculations are also described in the Supporting Information.

Supporting Information

Supporting Information is available from the Wiley Online Library or from the author.

Acknowledgements

This work was supported by the Mechanical Behavior of Materials Program (KC 13) at the Lawrence Berkeley National Laboratory, funded by the U.S. Department of Energy, Office of Science, Office of Basic Energy Sciences, Materials Sciences and Engineering Division, under Contract No. DE-AC02-05CH11231. A.W. was supported by an individual National Science Foundation Graduate Research Fellowship (Grant No. DGE 1106400). The authors would like to acknowledge Dr. Hao Bai, Dr. Benjamin Delattre, Yuyi Li, Bryanna Benicia, Brad Takasuka, and James Wu for their help with the experiments, and Dr. Ryan Wilkerson for his thoughtful discussion of the work.

Conflict of Interest

The authors declare no conflict of interest.

Keywords

bioinspired ceramics, ceramic–metal composites, compliant-phase ceramics, flexural strength, fracture toughness, nacre, spark plasma sintering

Received: January 30, 2019
Revised: April 24, 2019
Published online: May 27, 2019

[1] U. G. K. Wegst, H. Bai, E. Saiz, A. P. Tomsia, R. O. Ritchie, *Nat. Mater.* **2015**, *14*, 23.
[2] Z. Liu, M. A. Meyers, Z. Zhang, R. O. Ritchie, *Prog. Mater. Sci.* **2017**, *88*, 467.
[3] M. A. Meyers, P.-Y. Chen, A. Y.-M. Lin, Y. Seki, *Prog. Mater. Sci.* **2008**, *53*, 1.
[4] Y. A. Shin, S. Yin, X. Li, S. Lee, S. Moon, J. Jeong, M. Kwon, S. J. Yoo, Y.-M. Kim, T. Zhang, H. Gao, S. H. Oh, *Nat. Commun.* **2016**, *7*, 10772.
[5] S. E. Naleway, M. M. Porter, J. McKittrick, M. A. Meyers, *Adv. Mater.* **2015**, *27*, 5455.
[6] F. Barthelat, Z. Yin, M. J. Buehler, *Nat. Rev. Mater.* **2016**, *1*, 16007.
[7] M. Sarikaya, K. E. Gunnison, M. Yasrebi, I. A. Aksay, in *Materials Synthesis Utilizing Biological Processes: MRS Proc.* (Eds: P. C. Reieke, P. D. Calvert, M. Alper), Vol. *174*, Materials Research Society, Pittsburgh, PA **1990**, pp. 109–116.
[8] A. G. Evans, Z. Suo, R. Z. Wang, I. A. Aksay, M. Y. He, J. W. Hutchinson, *J. Mater. Res.* **2001**, *16*, 2475.
[9] B. L. Smith, T. E. Schäffer, M. Viani, J. B. Thompson, N. A. Frederick, J. Kindt, A. Belcher, G. D. Stucky, D. E. Morse, P. K. Hansma, *Nature* **1999**, *399*, 761.
[10] F. Song, A. K. Soh, Y. L. Bai, *Biomaterials* **2003**, *24*, 3623.
[11] G. X. Gu, F. Libonati, S. D. Wettermark, M. J. Buehler, *J. Mech. Behav. Biomed. Mater.* **2017**, *76*, 135.
[12] F. Barthelat, H. Tang, P. Zavattieri, C. Li, H. Espinosa, *J. Mech. Phys. Sol.* **2007**, *55*, 306.
[13] Fracture resistance can be considered as a mutual competition between two classes of toughening mechanisms: intrinsic mechanisms, which resist microstructural damage ahead of the crack tip and are motivated primarily by plasticity, and extrinsic mechanisms, which operate at, or in the wake of, the crack tip to inhibit fracture by "shielding" the crack from the applied driving force. Whereas intrinsic toughening mechanisms are effective in inhibiting both the initiation and growth of cracks, extrinsic toughening mechanisms, such as crack bridging and crack deflection, are only effective in inhibiting crack growth.
[14] Y. Shao, H.-P. Zhao, X.-Q. Feng, H. Gao, *J. Mech. Phys. Sol.* **2012**, *60*, 1400.
[15] H. Bai, A. Polini, B. Delattre, A. P. Tomsia, *Chem. Mater.* **2013**, *25*, 4551.

[16] H. Bai, F. Walsh, B. Gludovatz, B. Delattre, C. Huang, Y. Chen, A. P. Tomsia, R. O. Ritchie, *Adv. Mater.* **2015**, *28*, 50.
[17] H. Bai, Y. Chen, B. Delattre, A. P. Tomsia, R. O. Ritchie, *Sci. Adv.* **2015**, *1*, 1500849.
[18] S. Deville, E. Saiz, R. K. Nalla, A. P. Tomsia, *Science* **2006**, *311*, 515.
[19] V. Naglieri, H. A. Bale, B. Gludovatz, A. P. Tomsia, R. O. Ritchie, *Acta Mater.* **2013**, *61*, 6948.
[20] E. Munch, M. E. Launey, D. H. Alsem, E. Saiz, A. P. Tomsia, R. O. Ritchie, *Science* **2008**, *322*, 1516.
[21] P. M. Hunger, A. E. Donius, U. G. K. Wegst, *J. Mech. Behav. Biomed. Mater.* **2013**, *19*, 87.
[22] M. M. Porter, J. Mckittrick, M. A. Meyers, *JOM* **2013**, *65*, 720.
[23] A. Wat, J. I. Lee, C. W. Ryu, B. Gludovatz, J. Kim, A. P. Tomsia, T. Ishikawa, J. Schmitz, A. Meyer, M. Alfreider, D. Kiener, E. S. Park, R. O. Ritchie, *Nat. Commun.* **2019**, *10*, 961.
[24] P. Das, J.-M. Malho, K. Rahimi, F. H. Schacher, B. Wang, D. E. Demco, A. Walther, *Nat. Commun.* **2015**, *6*, 5967.
[25] F. Bouville, E. Maire, S. Meille, B. Van de Moortèle, A. J. Stevenson, S. Deville, *Nat. Mater.* **2014**, *13*, 508.
[26] G. Dwivedi, K. Flynn, M. Resnick, S. Sampath, A. Gouldstone, *Adv. Mater.* **2015**, *27*, 3073.
[27] S. Behr, U. Vainio, M. Müller, A. Schreyer, G. A. Schneider, *Sci. Rep.* **2015**, *5*, 9984.
[28] R. P. Wilkerson, B. Gludovatz, J. Watts, A. P. Tomsia, G. E. Hilmas, R. O. Ritchie, *Adv. Mater.* **2016**, *28*, 10061.
[29] R. P. Wilkerson, B. Gludovatz, J. Watts, A. P. Tomsia, G. E. Hilmas, R. O. Ritchie, *Acta Mater.* **2018**, *148*, 147.
[30] R. Libanori, R. M. Erb, A. R. Studart, *ACS Appl. Mater. Interfaces* **2013**, *5*, 10794.
[31] L. J. Bonderer, A. R. Studart, L. J. Gauckler, *Science* **2008**, *319*, 1069.
[32] R. M. Erb, R. Libanori, N. Rothfuchs, A. R. Studart, *Science* **2012**, *335*, 199.
[33] M. R. Begley, N. R. Philips, B. G. Compton, D. V. Wilbrink, R. O. Ritchie, M. Utz, *J. Mech. Phys. Sol.* **2012**, *60*, 1545.
[34] If the mortar strength does exceed the strength of the ceramic bricks, the bricks will simply fracture; this will immediately curtail the extrinsic toughening generated by crack bridging and brick pull-out, with the result that the structure will fracture catastrophically with a low toughness characteristic of the monolithic ceramic.
[35] E. Saiz, R. M. Cannon, A. P. Tomsia, *Annu. Rev. Mater. Res.* **2008**, *38*, 197.
[36] N. Eustathopoulos, *Metals* **2015**, *5*, 350.
[37] C. Garcia-Cordovilla, E. Louis, J. Narciso, *Acta Mater.* **1999**, *47*, 4461.
[38] X. Shen, M. Jing, W. Li, D. Li, *Powder Technol.* **2005**, *160*, 229.
[39] K. Nogi, N. Iwamoto, K. Ogino, *Trans. JWRI* **1992**, *21*, 141.
[40] N. Eustathopoulos, B. Drevet, M. L. Muolo, *Mater. Sci. Eng., A* **2001**, *300*, 34.
[41] B. R. Lawn, S. W. Freiman, T. L. Baker, D. D. Cobb, A. C. Gonzalez, *J. Am. Ceram. Soc.* **1984**, *67*, c67.
[42] J. J. Kruzic, R. M. Cannon, R. O. Ritchie, *J. Am. Ceram. Soc.* **2005**, *88*, 2236.
[43] P. Chantikul, S. J. Bennison, B. R. Lawn, *J. Am. Ceram. Soc.* **1990**, *73*, 2419.
[44] R. G. Munro, *J. Am. Ceram. Soc.* **1997**, *80*, 1919.
[45] Z. A. Munir, U. Anselmi-Tamburini, M. Ohyanagi, *J. Mater. Sci.* **2006**, *41*, 763.
[46] R. Orrù, R. Licheri, A. M. Locci, A. Cincotti, G. Cao, *Mater. Sci. Eng., R* **2009**, *63*, 127.
[47] Z. Xu, J. Huang, C. Zhang, S. Daryadel, A. Behroozfar, B. McWilliams, B. Boesl, A. Agarwal, M. Minary-Jolandan, *Adv. Eng. Mater.* **2018**, *20*, 1700782.
[48] H. L. Ferrand, F. Bouville, T. P. Niebel, A. R. Studart, *Nat. Mater.* **2015**, *14*, 1172.
[49] M. J. Garnier, D. C. Dunand, *Mater. Sci. Eng., A* **2019**, *743*, 190.
[50] ASTM Standard D790, *Standard Test Methods for Flexural Properties of Unreinforced and Reinforced Plastics and Electrical Insulating Materials*, ASTM International, West Conshohocken, PA **2017**.
[51] ASTM Standard E1820, *Standard Test Method for Measurement of Fracture Toughness*, ASTM International, West Conshohocken, PA **2016**.

